Polymer 55 (2014) 6915–6923

Contents lists available at ScienceDirect

Polymer

journal homepage: www.elsevier.com/locate/polymer

Structural evolution of β − iPP during uniaxial stretching studied by *in–situ* WAXS and SAXS

Chunbo Zhang, Guoming Liu*, Yan Song, Ying Zhao*, Dujin Wang

Beijing National Laboratory for Molecular Sciences, CAS Key Laboratory of Engineering Plastics, Institute of Chemistry, Chinese Academy of Sciences, Beijing 100190, China

ARTICLE INFO

Article history:
Received 30 June 2014
Received in revised form
19 September 2014
Accepted 26 October 2014
Available online 1 November 2014

Keywords:
β − nucleated isotactic polypropylene (β − iPP)
Orientation
Crystal transition

ABSTRACT

Polymorphism and crystal transition are of great significance for property mediation in polymer materials. Isotactic polypropylene (iPP) with β − crystal has been widely utilized for the preparation of high performance plastics or films. In the present work, the structural evolution of initially isotropic β − nucleated iPP (β − iPP) during uniaxial stretching at different temperatures was investigated by *in–situ* X − ray scattering using synchrotron radiation. The wide − angle X − ray scattering (WAXS) results confirmed that the β − crystal transformed either to the mesophase at lower temperature (30 °C) or to the α − crystal at higher temperature (60, 100 and 120 °C) during stretching. An interesting orientation of β − crystal with molecular chains perpendicular to the tensile direction was identified. As revealed by small − angle X − ray scattering (SAXS), cavitation took place in β − iPP stretched at temperatures lower than 120 °C. The size and shape of the cavities were observed by scanning electron microscope. A deformation mechanism of β − iPP combining the crystal transition, cavitation and orientation was proposed.

1. Introduction

As a typical semicrystalline polymer, the properties of isotactic polypropylene (iPP) are largely determined by the crystalline phase including the crystal form and morphology. To date, three crystal modifications (α, β and γ) and a mesophase have been identified in iPP. Molecular chains adopt a 3_1 helical conformation in the four phases [1–5]. The monoclinic α − form is thermodynamically the most stable one, which is found under ordinary processing conditions. The β − crystal, with trigonal unit cell ($a = b = 11.03$ Å, $c = 6.50$ Å, $\gamma = 120°$) [6,7], can be obtained under certain conditions: crystallization induced by β − nucleating agents [1,8,9], under shear [10], or under gradient temperatures [11]. Interestingly, applying shear flow on iPP melt containing β − nucleating agent yielded lower β − crystal content compared with quiescently crystallized sample [12–14]. The β − crystal spherulites exhibit bundled radial lamellar arrangement and display inherently higher ductility than the cross − hatched α − spherulites [1,15]. Therefore iPP crystallized predominately in β − crystal (designated as β − iPP, hereafter) shows improved mechanical properties, including enhanced impact toughness and higher heat deflection temperature [16,17], which makes β − crystal especially attractive for numerous studies.

The deformation mechanism of semicrystalline polymers is a traditional but long − disputed topic. At the very early stage, the deformation is essentially elastic, coming from the crystalline skeleton [18–21] and amorphous phase [22,23]. Approaching macroscopic yield point, crystallographic slips or intralamellar mosaic blocks slips start to proceed [22,24]. At large strains, stress − induced fragmentation/recrystallization dominates, resulting in an oriented fibrillar structure [25]. Tensile deformation of semicrystalline polymers is frequently accompanied by cavitation, such as in iPP [26–28], high − density polyethylene and poly(methylene oxide) [29]. Cavities may be initiated first in amorphous regions [29] or in crystalline phase [21,30]. Galeski and Bartczak [31] proposed that cavitation appeared to be another mechanism of tough response of materials.

To understand the mechanical enhancement imparted by β − crystal, the deformation behavior and associated structural evolution of β − iPP have been investigated extensively [32–38]. Two major focuses are crystal transition and cavitation during deformation. β − crystal is unstable and can transform either to the mesophase or to the α − crystal after yielding depending on deformation temperature [33–36]. Cai et al. [33] found that the initial engineering strain for β − α transformation decreased with stretching

* Corresponding authors.
E-mail address: gmliu@iccas.ac.cn (G. Liu).

http://dx.doi.org/10.1016/j.polymer.2014.10.049
0032-3861/

temperature. The nature of the stress – induced crystal transition in β – iPP was ascribed to partial melting – recrystallization [32,39] or solid – solid martensitic transformation [34], which is still not very clear. On the other hand, β – iPP exhibits more pronounced cavitation during stretching compared with α – iPP [40]. This feature has been using to fabricate high permeability microporous membranes [41]. Chu et al. [42] suggested that the cavity formation in β – iPP was induced by volume contraction during β – α transformation. However, Ran et al. [43] proposed that cavities in β – iPP might be initiated at the defect point under stress.

Most of the previous reports paid much attention on the content of different phases, critical strain/temperature and cavitation in the deformation process of β – iPP. However, the orientation of β – crystal during uniaxial stretching is of less focus. A systematic understanding of the correlation among crystal transition, orientation and cavitation is still limited. In this work, β – iPP samples were isothermally crystallized from the melt to eliminate any possible preexisting orientation. The uniaxial tensile deformation process was investigated by *in–situ* small – angle and wide – angle X – ray scattering (SAXS/WAXS) at various temperatures (30, 60, 100 and 120 °C). A deformation mechanism of β – iPP based on the relationship among crystal transition, orientation and cavitation was proposed.

2. Experimental section

2.1. Materials

The iPP (S1003) with melt flow rate (MFR) = 3.4 g/10 min at 230 °C/2.16 kg was supplied by SINOPEC Beijing Yanshan Company. Calcium pimelate (Ca – Pim), a β – nucleating agent, was synthesized by neutralization reaction of pimelic acid (Sigma – Aldrich) and $Ca(OH)_2$ (Xilong Chemical Co., Ltd.) in deionized water at 80 °C.

2.2. Sample preparation

iPP pellets were mixed with Ca – Pim powder using an internal mixer (HAAKE Rheomix OS) at 200 °C for 6 min with a rotating speed of 50 rpm. The weight fraction of β – nucleating agent was 0.1%. Compounded iPP plaques were prepared by compression molding at 230 °C. The samples were melted at 230 °C for 5 min and then cooled to the crystallization temperature of 125 °C on a Linkam LTS350 hotstage (Linkam Scientific Instruments, Ltd., U.K.). After being annealed for 60 min, the plaques were cooled to room temperature at a rate of 30 °C/min. Mini tensile bars about 1 mm thick were cut from the plaques.

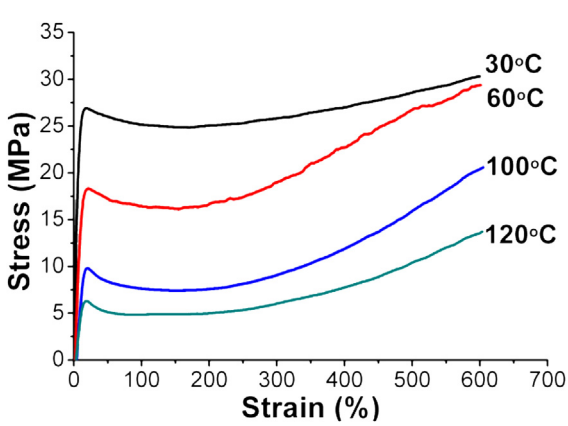

Fig. 1. Engineering stress – strain curves of β – iPP at different temperatures. The opening velocity of the clamp is 3.0 mm/min.

2.3. In–situ synchrotron X – ray measurements

In–situ X – ray measurements were carried out at the beamline BL16B1 in the Shanghai Synchrotron Radiation Facility (SSRF). The wavelength of the radiation was 0.124 nm. The mini tensile bars were stretched on a Linkam TST350 tensile hotstage at 30, 60, 100 and 120 °C, respectively. Once the temperature reached the target value at a rate of 30 °C/min, the sample was equilibrated for 2 min and then stretched at a constant speed of 3.0 mm/min. The structure information was recorded by WAXS and SAXS *in–situ*. All the scattering patterns were collected by a MAR CCD (MAR – USA) detector with a resolution of 2048 × 2048 pixels and pixel size of 79 × 79 μm^2. Image acquisition time was 15 s for WAXS and 1 s for SAXS. The sample to detector distance was 194 mm for WAXS and 2074.7 mm for SAXS. The scattering patterns were corrected for background scattering, air scattering and beam fluctuations.

2.4. Scanning electron microscope (SEM)

The morphology of the cryo – fractured surface along the stretching direction of deformed β – iPP was observed on a JSM – 6700F JEOL SEM, operated at an accelerating voltage of 5 kV. All samples were gold sputtered prior to the SEM characterization.

3. Results and discussion

3.1. Stress – strain curves of β – iPP at different temperatures

The engineering stress – strain curves of β – iPP are shown in Fig. 1. The samples exhibit ductile behavior with typical elastic region, yielding, strain softening and strain hardening. The yield

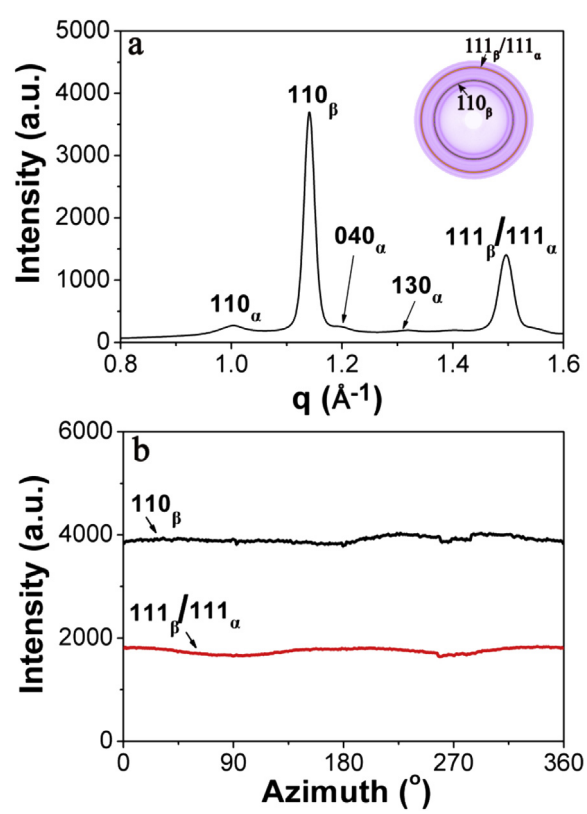

Fig. 2. (a) Indexed 1D WAXS intensity profile of unstretched β – iPP at room temperature (inset shows 2D pattern). The scattering vector is defined as $q = 4\pi \times \sin\theta/\lambda$, in which θ is the half Bragg angle, and λ is the wavelength of the radiation. (b) Azimuthal intensity distribution of 110_β and $111_\beta/111_\alpha$.

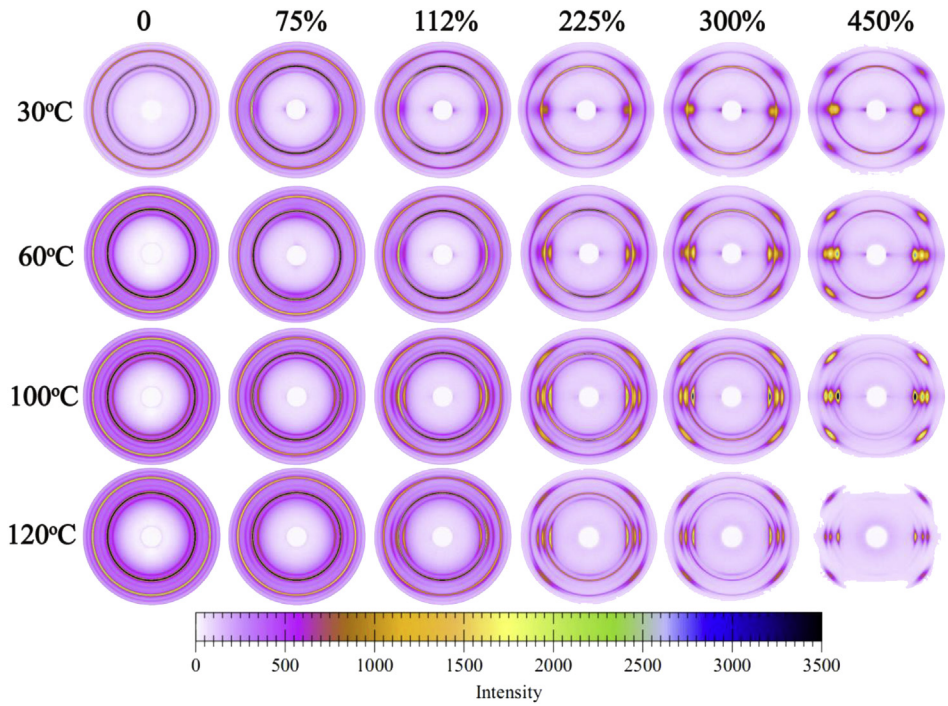

Fig. 3. Selected WAXS patterns of $\beta-$ iPP during tensile deformation at different temperatures. The drawing direction is vertical.

stress decreases from 27 MPa at 30 °C to 6 MPa at 120 °C. It has been known that chain mobility is important for the ductile behavior of polymers [44]. Semicrystalline polymers show softer overall mechanical response at elevated temperatures.

3.2. Crystalline structure of unstretched $\beta-$ iPP

Fig. 2a shows the 1D WAXS intensity profile of unstretched $\beta-$ iPP. The two strongest diffraction peaks correspond to 110_β and $111_\beta/111_\alpha$, from low to high q, respectively. The 2D scattering pattern has been averaged over 360° to obtain 1D intensity profile. Several weak peaks originating from $\alpha-$ form can be indexed as the 110_α, 040_α, 130_α and 111_α planes with $d-$ spacing of 6.25, 5.18, 4.76 and 4.16, respectively. The fraction of $\beta-$ crystal in the unstretched sample is about 55% estimated by the ratio of integrated intensity of $\beta-$ crystal and the total integrated intensity. According to characterizing parameter proposed by Turner – Jones et al. [45], k_β value is defined as follows:

$$k_\beta = \frac{A(110_\beta)}{A(110_\beta)+A(110_\alpha)+A(040_\alpha)+A(130_\alpha)}$$

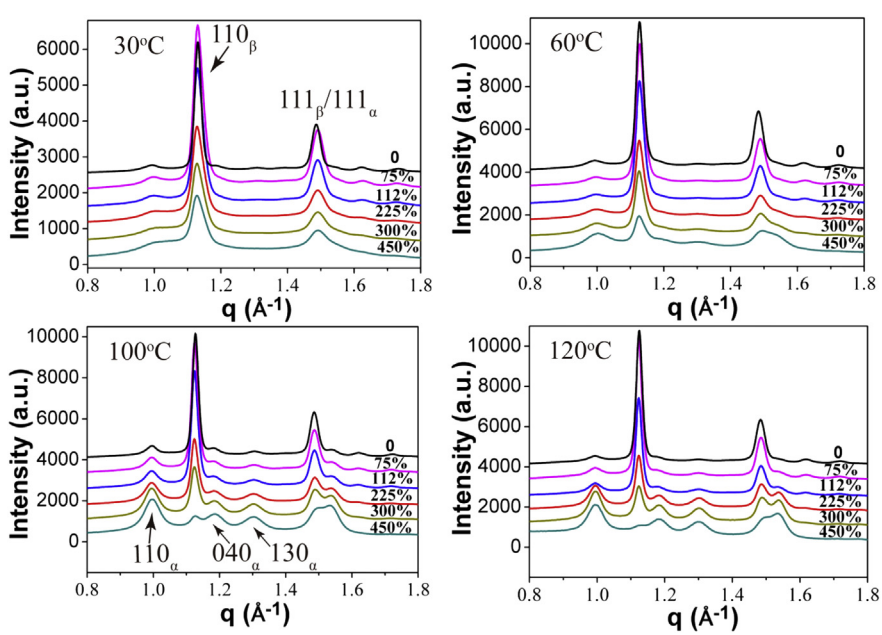

Fig. 4. 1D intensity profiles obtained from circularly integrated intensities (from 0 to 360°) of 2D WAXS patterns of $\beta-$ iPP as a function of strain at different temperatures.

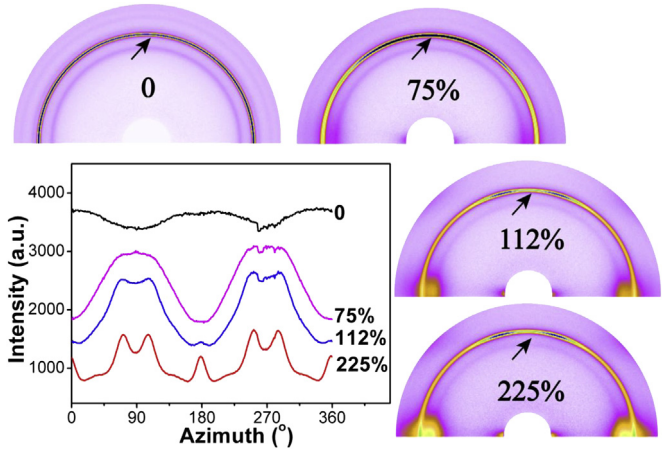

Fig. 5. Azimuthal intensity distribution of 110_β reflection of $\beta-$ iPP (indicated by the arrows) as a function of strain at 30 °C. The drawing direction is vertical.

where $A(110_\alpha)$, $A(040_\alpha)$ and $A(130_\alpha)$ are the areas of the three strongest $\alpha-$ form peaks, and the $A(110_\beta)$ is the area of the strongest $\beta-$ crystal peak. The k_β of the $\beta-$ iPP used in this study is 0.9, which is a very high value. The azimuthal intensity distribution of 110_β and $111_\beta/111_\alpha$ is plotted in Fig. 2b. The flat shape indicates that the distribution of the orientation of β crystallites is perfectly random. This provides a basis for orientation analysis of $\beta-$ crystal during stretching.

3.3. In–situ wide – angle X – ray scattering (WAXS) of $\beta-$ iPP under stretching

The WAXS patterns of $\beta-$ iPP during tensile deformation at different temperatures are presented in Fig. 3. Upon deformation, the azimuthal distribution of reflection rings becomes less uniform. Stretching at 30 °C, two broad spots appear on the equator, and four spots emerge on the off – equatorial region when the strain reaches 225%. This corresponds to the feature of mesophase [46]. When stretching at higher temperatures, the reflections corresponding to $\alpha-$ crystal turn to be stronger, as shown in Fig. 4. The new phases transformed from $\beta-$ crystal are anisotropic with chain parallel to the drawing direction. It can be seen that $\beta-$ crystal transforms to mesophase at 30 °C, and transforms mainly to $\alpha-$ crystal at 100 and

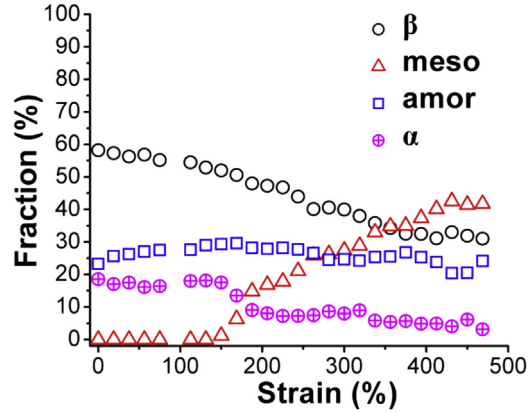

Fig. 7. Fractions of different phases in $\beta-$ iPP during tensile deformation at 30 °C.

120 °C. Both mesophase and $\alpha-$ crystal are observed in $\beta-$ iPP deformed at 60 °C. The overall feature of crystal transition is in line with the previous reports [33,36,47]. It is worthy to notice that the final content of $\beta-$ crystal depends strongly on stretching temperature. At strain = 450%, a large amount of $\beta-$ crystal still remains at 30 °C. On the other hand, the reflection of $\beta-$ crystal totally vanishes stretched at 120 °C. More quantitative analysis will be addressed below.

Fig. 5 shows the azimuthal distribution of 110_β reflection of $\beta-$ iPP at different strains stretched at 30 °C, the orientation and crystal transition of $\beta-$ crystal can be observed. Pawlak reported that the 110_β ring was always uniform during deformation [40], which is obviously not the case in our studies. It should be borne in mind that orientation and crystal transition are two coupled processes. The complex structural evolution reflects the fine details of the crystal transition. Upon deformation, the intensity on the equator decreases, leaving the arcs on the meridian (azimuth = 90°, 270°). At strain = 112%, the meridian arc splits into two parts. Upon further deformation, two equatorial peaks emerge (azimuth = 0°, 180°).

In order to characterize the complex crystal transition during deformation, a quantitative analysis on the phase contents is necessary. Because of the severe overlapping of several peaks of different phases, estimation using conventional peak fitting method would cause unacceptably large uncertainties. To calculate the fractions of phases accurately, we adopted a data treatment

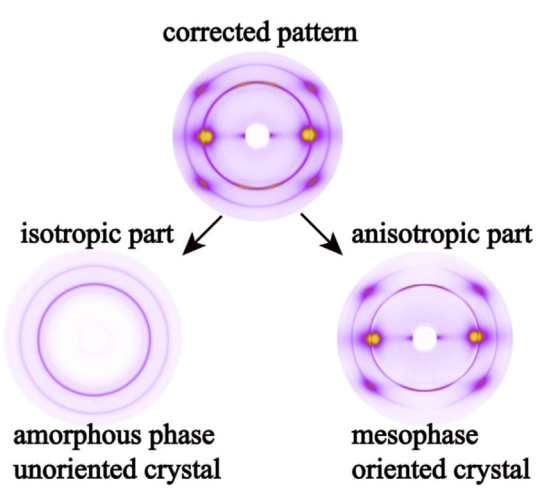

Fig. 6. An example showing the separation of a WAXS pattern into the isotropic and anisotropic parts. The stretching temperature is 30 °C, and the strain is 450%.

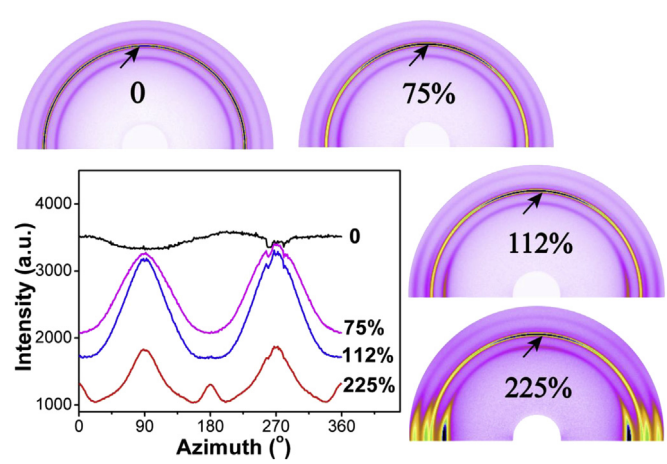

Fig. 8. Azimuthal intensity distribution of 110_β reflection of $\beta-$ iPP (indicated by the arrows) as a function of strain at 100 °C. The drawing direction is vertical.

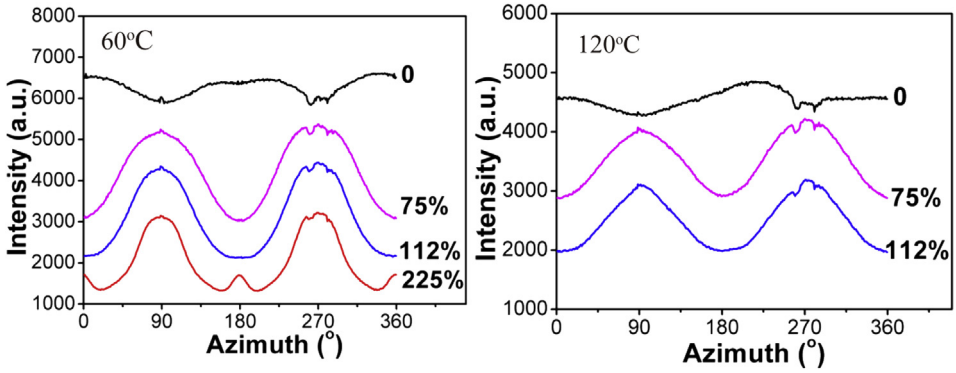

Fig. 9. Azimuthal intensity distribution of 110_β of $\beta-$ iPP as a function of strain at 60 and 120 °C. The intensity of 110_β at strain = 225% in $\beta-$ iPP deformed at 120 °C is too weak, so it is not presented.

method ("halo method") [48,49]. As shown in Fig. 6, the isotropic part mainly contains the amorphous phase and unoriented crystalline phase, whereas the anisotropic part is constituted by mesophase and oriented crystalline phase. For $\beta-$ iPP, the 1D profile of the isotropic part was fitted by nine Gaussian + Lorentz type peaks: two $\beta-$ crystal peaks, two amorphous peaks, and five $\alpha-$ crystal peaks. The anisotropic part was also fitted by nine Gaussian + Lorentz type peaks: two $\beta-$ crystal peaks, two mesophase peaks and five $\alpha-$ crystal peaks. The center positions of $\beta-$ crystal peaks, amorphous peaks, $\alpha-$ crystal peaks and mesophase peaks were fixed during parameter optimization [10,48].

Fig. 7 shows the fractions of different phases of $\beta-$ iPP during stretching at 30 °C. Up to strain = 100%, no mesophase could be detected. Upon strain further increasing to 475%, the fraction of $\beta-$ crystal decreases smoothly from ~55% to ~35%, and the content of $\alpha-$ crystal decreases from ~25% to ~5%. Meanwhile, the fraction of mesophase increases from 0 to ~ 45%. This indicates that the mesophase derives from both β and $\alpha-$ crystal, in accordance with the previous report [49]. The fraction of amorphous phase nearly keeps constant during deformation.

The azimuthal distribution of 110_β reflection at 100 °C is shown in Fig. 8. As the strain increased, the intensity on the equator decreases similar to the results at 30 °C. At strain = 225%, two equatorial maxima can be seen. Different from the results at 30 °C, no splitting of the meridian arcs are observed. The orientation behavior of $\beta-$ crystal at tensile temperature of 60 and 120 °C (shown in Fig. 9) is similar to that at 100 °C. Similar to the data treatment method of 30 °C, the quantitative analysis on the phase contents and crystal transition process for $\beta-$ iPP at 100 °C is shown in Fig. 10. Upon strain increasing, the fraction of $\beta-$ crystal decreases from ~55% to ~5%. Meanwhile, the fraction of $\alpha-$ crystal increases from ~20% to ~85%. The fraction of amorphous phase is almost unchanged.

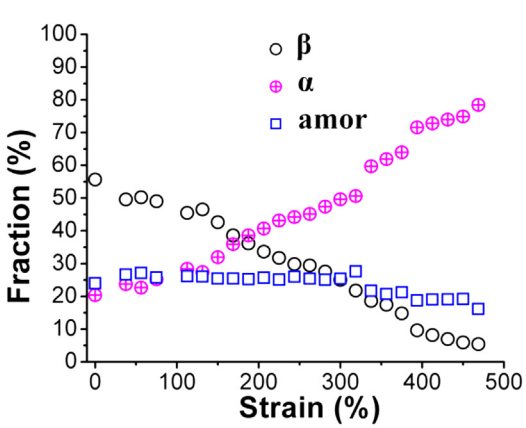

Fig. 10. Fractions of different phases in $\beta-$ iPP during tensile deformation at 100 °C.

3.4. In–situ small – angle X – ray scattering (SAXS)

SAXS is a powerful tool to characterize cavitation in polymer, as the high contrast between cavity and polymer matrix. Fig. 11 presents the selected SAXS patterns of $\beta-$ iPP at different temperatures during tensile deformation. In the unstretched state, $\beta-$ iPP shows relatively weak but uniform scattering ring, corresponding to isotropic lamellae stacks in the unstretched samples. The scattering intensity has a drastic increase stretched at 30 °C (strain = 10%). The scattering intensity on the meridian is much stronger than that on the equator, indicating the occurrence of cavitation and the cavities are elongated preferentially perpendicular to the drawing direction. When strain = 50%, the intensity on the equator becomes comparable with that on the meridian. With strain further increasing, the scattering intensity on the equator keeps increasing, while the intensity on the meridian decreases. This implies the reorientation of cavities. At high strains, the cavities are elongated along the stretching direction. Similar phenomena are observed for $\beta-$ iPP deformed at 60 and 100 °C. It can be noticed that the onset engineering strain for cavitation in $\beta-$ iPP becomes higher when stretched at higher temperatures. No cavity scattering signal can be detected during stretching at 120 °C.

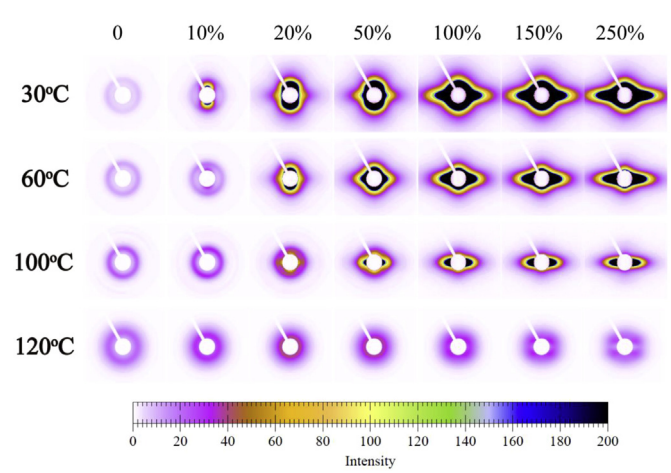

Fig. 11. SAXS patterns of $\beta-$ iPP stretched at different temperatures. The drawing direction is vertical.

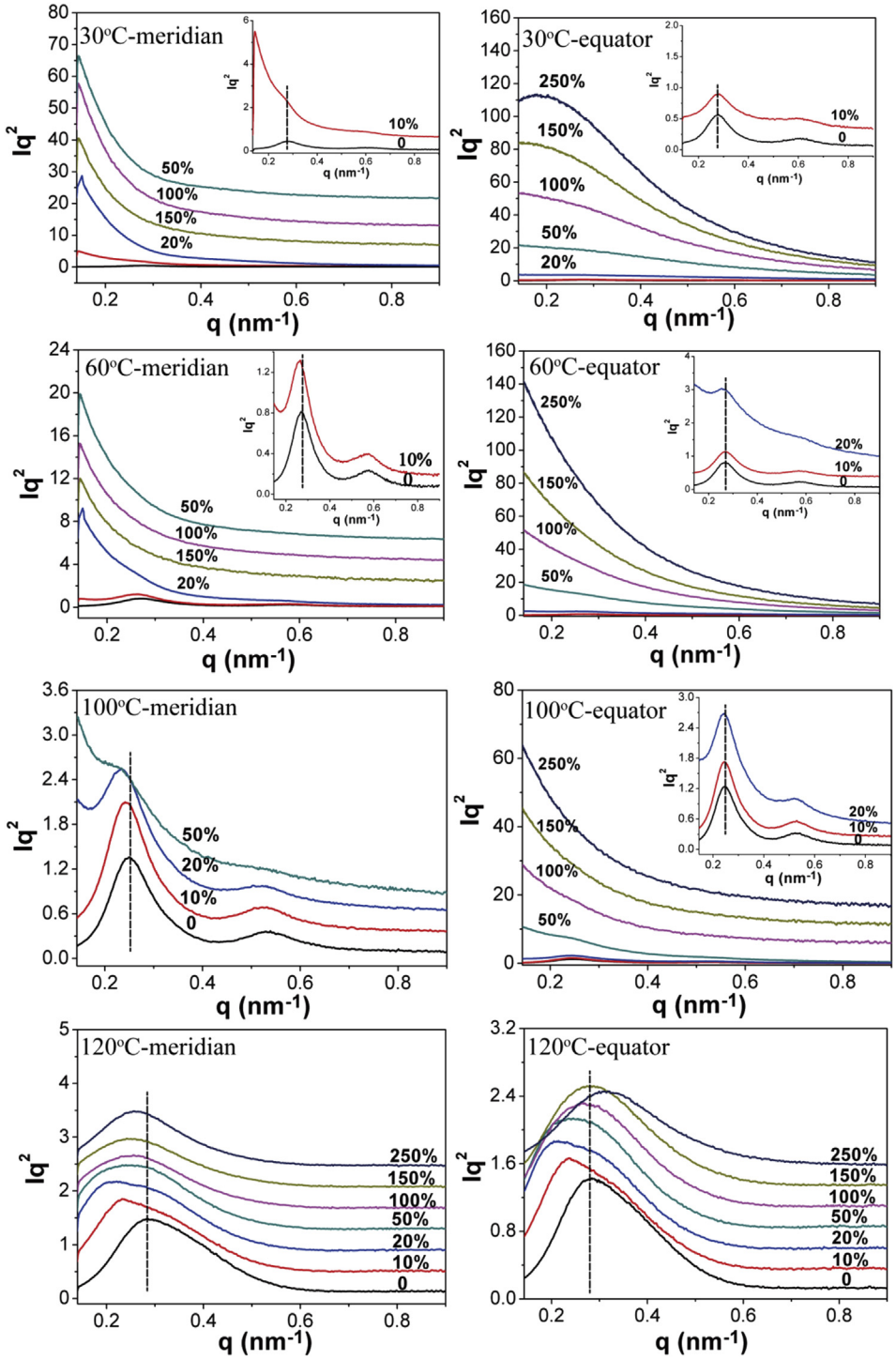

Fig. 12. Lorentz corrected 1D SAXS profiles of deformed $\beta-$ iPP along the meridian and equator at different temperatures. q is the scattering vector.

Although the cavitation of $\beta-$ iPP has been reported previously [33,36], a systematic investigation on the effect of temperature on the cavitation of $\beta-$ iPP is firstly shown here.

The formation of cavities and the change of long period in $\beta-$ iPP during tensile deformation can be further confirmed by the 1D SAXS meridional and equatorial profiles (Fig. 12). Two diffraction maxima are observed in the unstretched samples at 30, 60 and 100 °C. The peak positions move to lower q with temperature increasing. The low q peak arises from the Bragg diffraction of periodic lamellae. The long period is defined as the average distance between adjacent lamellae, and can be estimated by $L = 2\pi/q_{max}$, in which q_{max} is the q value at the peak maximum [50]. The existence of second order peak indicates that the packing of $\beta-$ iPP lamellae is regular. Only a broad peak is observed at 120 °C with $q_{max} = 0.28$ nm^{-1}, which is much broader than those at lower temperatures. This feature indicates that the regularity of lamellae packing becomes less ordered. This may be caused by the partial melting of β lamellae.

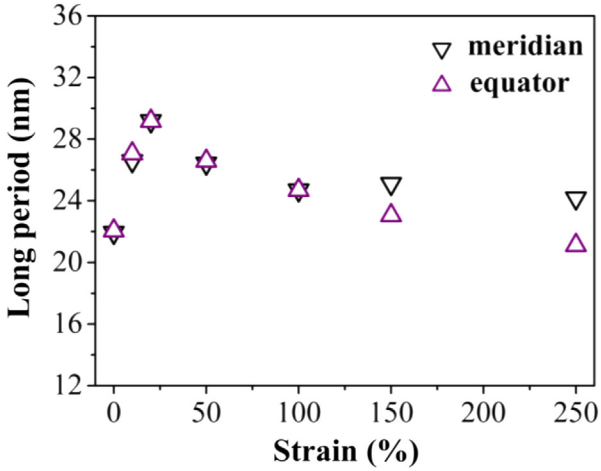

Fig. 13. The long periods of β − iPP as a function of strain stretched at 120 °C along the meridian and the equator.

Similar regulation is observed for stretching at 30, 60 and 100 °C. Upon stretching, the peak position along the meridian moves to lower q, while the equatorial q_{max} is almost unchanged. Compared with the deformation of polyethylene (PE) and its copolymers, the change of long period of our samples is less obvious [51,52]. As the strain reaches 10%, the cavitation signal appears and dominates. Gradually, the long period scattering is covered by the scattering of cavities. The intensity on the meridian reaches its maximum at strain = 50%, while the intensity on the equator increases upon deformation. Dramatic differences are noticed in the sample stretched at 120 °C. The long period peak is always visible during stretching. The long period is plotted as a function of strain, as shown in Fig. 13. The increase of long period along the meridian is associated with the interlamellar separation under tension. The subsequent decrease of the long period corresponds to the rearrangement of the lamellae, producing an oriented superstructure. The long period along the equator varies in a similar manner. This is quite uncommon compared with other polymers, such as α − iPP [53,54], polyethylene [55], ethylene − propylene copolymers [56], etc., in which the equatorial long period either decreases or keeps unvaried during initial deformation.

To get more direct information about the cavities in β − iPP, the cryo − fractured cross section was observed by SEM, as shown in Fig. 14. The engineering strain for all the samples is 250% for comparison. Clear differences can be seen between samples deformed at different temperatures. The average size of cavities increases with stretching temperature increasing. The cavities in β − iPP deformed at 30 °C have the smallest aspect ratio, while the cavities for 100 °C are highly elongated. Most of the cavities connect with each other and contain fibrils.

The increase of tensile temperature changes the intrinsic properties of crystalline/amorphous phases in β − iPP. Cavitation takes place in drawn polymers in which the level of stress necessary for inducing cavitation lower than the value required for crystal plastic deformation [29]. The crystals become less rigid as temperature increased. This can be reflected macroscopically by the reduction of yield stress at a higher temperature. Plastic deformation of crystals is easier to initiate at an elevated temperature. A number of factors influence the intensity of cavitation besides temperature [57], such as lamellar thickness, orientation [29,58], interlamellar thickness [27], polymer molecular weight and strain rate [26,59]. It is not surprising that cavities were observed in β − iPP at tensile temperature as high as 130 °C in another study [36].

3.5. Deformation mechanism

Many studies have been carried out focusing on different aspects of the deformation process of β − iPP, e.g. crystal transition, cavitation and fracture behavior. However, the understanding on how these complicated processes couple with each other is still limited. By combination of WAXS and SAXS, it is possible to obtain some in − depth insights. Several aspects are discussed in detail below.

(a) Crystal transition. Similar to previous studies [32,33], the crystal transition took place after yielding, in company with plastic deformation. And the onset engineering strain decreased with stretching temperature increasing. In our case, the β − mesophase transition was observed at 30 °C, and the β − α transition was observed at 60, 100 and 120 °C. The variation trends of different phases were affected by the drawing temperature. This can be attributed to the different stability of different phases. According to Zannetti et al. [60], iPP mesophase transforms to α − crystal annealed at 60 °C, indicating the stability up limit for mesophase is 60 °C. In addition, the final content of β − crystal before fracture decreased with stretching temperature increasing. Stretched at 120 °C, no β − crystal can be observed at high strains.

As mentioned, the chain conformations in α, β and mesophase are identical (3_1 helix) [1–4]. The α − crystal has a unit cell with layers made of isochiral helices parallel to the *ac* plane, but the alternate layers are antichiral. Chains in β − crystal unit cell have isochiral helices. The helix chiralities are random in mesophase formed through deformation [48]. The stress − induced crystal transition from ordered α or β phase to the disordered mesophase

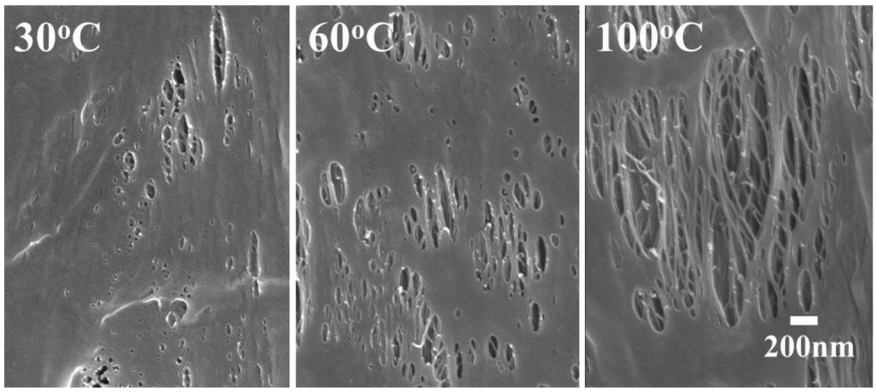

Fig. 14. SEM images of drawn β − iPP with an engineering strain of 250% at different temperatures. The drawing direction is vertical.

was proposed to be achieved by recrystallization of the pulled out chains [5,32,39,61,62]. On account of different helix chiralities of β − crystal and α − crystal, the β −α transition should experience a local melting and recrystallization process. It should be noted that the "melting" induced by stress [25] may be quite different from normal thermal melting. The high stretching temperature made the transition easier by facilitating the "melting" of β − crystal.

(b) Cavitation. Cavities were observed in β − iPP stretched at temperatures below 120 °C in our study. But in other studies [33,36], cavitation can be detected above 120 °C. The onset engineering strain for cavitation becomes higher as the temperature increased. At the beginning, cavities were oriented perpendicular to the stretching direction. Shortly afterwards, the reorientation of cavities took place, i.e. the cavities were elongated along the tensile direction at high strains. The size and shape of cavities were different in deformed β − iPP at different stretching temperatures.

As the strain reaches 10% at 30 °C, cavitation takes place, but the crystal transition does not occur simultaneously. On the other hand, cavitation is not observed at 120 °C when the β − α transformation still exists. This indicates that the crystal transition and the cavitation are two independent phenomena in the stretching process of β − iPP. Thus the crystal transition cannot be the sole reason for cavitation in β − iPP. The mechanism of cavitation in β − iPP may be similar to that in α − iPP. Cavities can be observed when the negative pressure generated by stress higher than the value required for cavitation [29]. However, as a stress releasing process, cavitation does have influence on the crystal transition. Cavitation becomes less pronounced at higher stretching temperature. Correspondingly the final content of β phase before fracture decreases with stretching temperature increasing.

(c) Orientation of β − crystal. The most interesting phenomenon is the orientation of β − crystal. And this orientation of residual β − crystal can provide microscopic clues to correlate the relationship of deformation and crystal transition. Generally, tensile deformation will produce an oriented structure with chain axis aligned preferentially along the stretching direction [22]. To understand the structural evolution of the β − crystal, a schematic illustration of the deformation process of β − iPP during uniaxial stretching is presented in Fig. 15. It should be pointed out that the reorientation of cavities is a universal phenomenon in all our studied samples with cavitation, therefore the structure with cavities perpendicular to the stretching direction is omitted in the illustration.

Before yielding, the deformation mainly includes interlamellar slip, interlamellar separation and stack rotation. As plastic deformation proceeds, the lamellae with chain direction parallel to the drawing direction are gradually consumed by transforming to mesophase or α − crystal [47], as shown in Fig. 15 stage I. Therefore the intensity of 110_β on the equator is weaker than that on the meridian. The β − crystal lamellae with long axis parallel to the drawing direction survive. As a consequence, the chains of residual β − crystal are approximately perpendicular to the tensile direction. Upon strain further increasing (at stage II in Fig. 15), the β − crystal lamellae fragmented into smaller crystals. Parts of the residual β − crystal blocks tend to rotate to their favorable orientation, i.e. chains are parallel to the drawing direction. When the strain reaches 450%, orientation of β − crystal cannot be accurately measured due to the low fraction of β − crystal, especially at higher tensile temperatures (at stage III in Fig. 15).

Another interesting thing is that two off − meridian arcs are observed for 110_β reflection in β − iPP stretched at 30 °C. However, the 110_β reflection only exhibits one arc on the meridian at higher temperatures. The reflection splitting may originate from crystal twinning or tilting. The twinning can be proved by the orientation of crystal faces correlated with the twinning plane [63]. But only

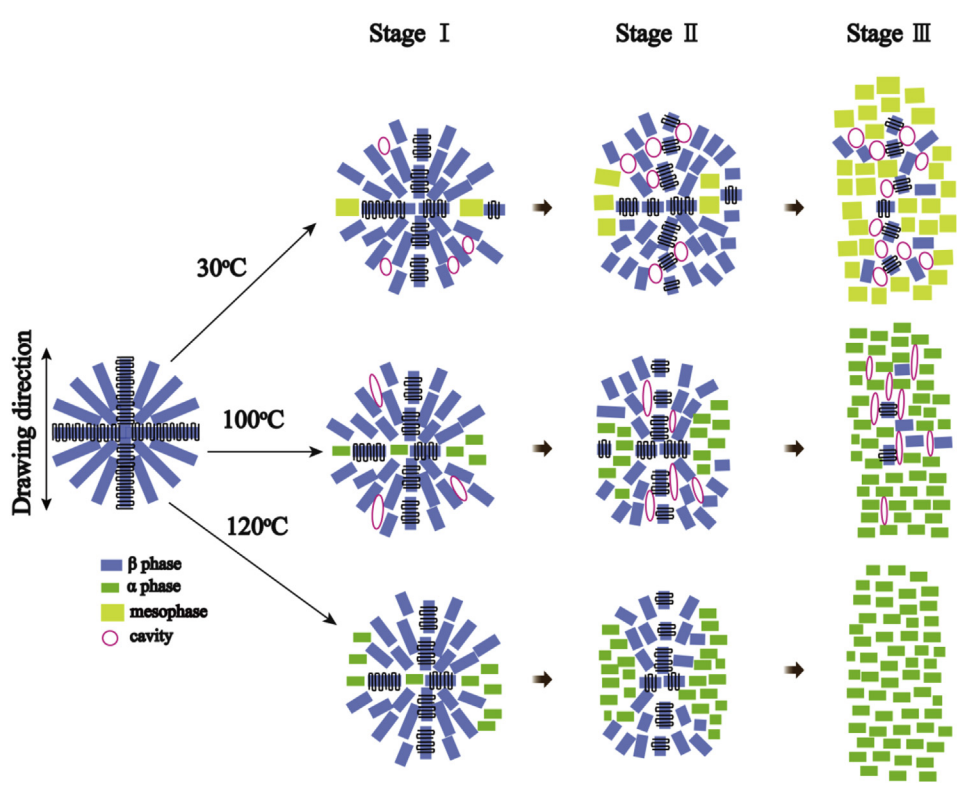

Fig. 15. Schematic illustration of the deformation process of β − iPP during uniaxial stretching at different temperatures. Stage I represents structure just after yielding, stage II represents the structure at a middle strain (~200%), and stage III indicates the structure just before fracture. The initial structure with cavities perpendicular to the stretching direction is omitted and the relative sizes of the spherulites, lamellae and cavities are not completely consistent with that of real structure in this illustration.

110_β and 111_β reflections of $\beta-$ crystal can be observed in 2D WAXS patterns of our sample, and the 111_β is overlapped with 111_α reflection. So it is difficult to provide the direct evidence on the occurrence of twinning. Therefore we try to use the tilting of lamellae to explain the reflection splitting.

Cavitation affects the orientation of crystallites. For example, cavitation with or without reorientation resulted in different orientation behavior in polybutene–1 [30]. In our case reorientation of cavities is always observed as long as cavitation occurs. As a stress releasing process, cavities produce a stress dissipation zone accommodating the residual $\beta-$ crystal, and possibly in such a way influence the orientation of $\beta-$ crystal. The shape of the cavities at 30 °C is roughly spherical, which may favor the two populations of tilted lamellae. As shown in Fig. 15 stage II (30 °C), the residual $\beta-$ lamellae with chain axis perpendicular to the stretching direction near the spherical cavities may tilt favorably, resulting in the two – arc pattern. When the stretching temperature is higher, the cavities are highly elongated (stage II at 100 °C) or do not exist (stage II at 120 °C). In these cases, those residual $\beta-$ lamellae do not necessarily have to tilt, therefore one – arc pattern is observed.

4. Conclusions

This study examined the uniaxial tensile deformation process of isotropic $\beta-$ iPP at different temperatures using *in–situ* X–ray scattering. Crystal transition and orientation of $\beta-$ crystal coupled with cavitation are observed during stretching. The $\beta-$ mesophase transition occurs at 30 °C, while $\beta-\alpha$ transition takes place at 60, 100 and 120 °C. On the other hand, cavitation is observed in $\beta-$ iPP when stretched at 30, 60 and 100 °C. As the tensile temperature reaches 120 °C, no cavities can be detected. Both $\beta-$ mesophase and $\beta-\alpha$ transition are believed to be achieved by melting and recrystallization. The crystal transition causes an interesting orientation of $\beta-$ crystal with molecular chains preferentially perpendicular to the tensile direction. The cavitation plays a role in influencing the crystal transition and lamellar orientation in deformed $\beta-$ iPP by dissipating the stress and accommodating the residual β crystallites.

Acknowledgments

Financial support from the National Natural Science Foundation of China (NSFC, Grant No. 51203170) is gratefully acknowledged. The SSRF is acknowledged for kindly providing the beam time.

References

[1] Varga J. J Macromol Sci B 2002;41:1121–71.
[2] Lotz B, Wittmann JC, Lovinger AJ. Polymer 1996;37(22):4979–92.
[3] Meille SV, Bruckner S. Nature 1989;340(6233):455–7.
[4] Androsch R, Di Lorenzo ML, Schick C, Wunderlich B. Polymer 2010;51(21):4639–62.
[5] Saraf R, Porter RS. Mol Cryst Liq Cryst Lett 1985;2(3–4):85–93.
[6] Meille SV, Ferro DR, Briuckner S, Lovinger AJ, Padden FJ. Macromolecules 1994;27:2615–22.
[7] Dorset DL, Mccourt MP, Kopp S, Schumacher M, Okihara T, Lotz B. Polymer 1998;39(25):6331–7.
[8] Shi GY, Zhang XD, Qiu ZX. Die Makromol Chem 1992;193(3):583–91.
[9] Li C, Su DF, Su ZQ, Chen XN. Chin J Polym Sci 2014;32(9):1167–75.
[10] Somani RH, Hsiao BS, Nogales A, Fruitwala H, Srinivas S, Tsou AH. Macromolecules 2001;34(17):5902–9.
[11] Lovinger AJ, Chua JO, Gryte CC. J Polym Sci Pol Phys Ed 1977;15(4):641–56.
[12] Chen YH, Mao YM, Li ZM, Hsiao BS. Macromolecules 2010;43(16):6760–71.
[13] Huo H, Jiang S, An L, Feng J. Macromolecules 2004;37(7):2478–83.
[14] Chen YH, Zhong GJ, Wang Y, Li ZM, Li L. Macromolecules 2009;42(12):4343–8.
[15] Aboulfaraj M, Sell CG', Ulrich B, Dahoun A. Polymer 1995;36(4):731–42.
[16] Varga J, Ehrenstein G. Beta-modification of isotactic polypropylene. In: Karger-Kocsis J, editor. Polypropylene, vol. 2. Netherlands: Springer; 1999. p. 51–9.
[17] Chen HB, Karger-Kocsis J, Wu JS, Varga J. Polymer 2002;43:6505–14.
[18] Hiss R, Hobeika S, Lynn C, Strobl G. Macromolecules 1999;32(13):4390–403.
[19] Men Y, Strobl G. Macromolecules 2003;36(6):1889–98.
[20] Men Y, Rieger J, Strobl G. Phys Rev Lett 2003;91(9):095502.
[21] Men Y, Rieger J, Homeyer J. Macromolecules 2004;37(25):9481–8.
[22] Bowden PB, Young RJ. J Mater Sci 1974;9(12):2034–51.
[23] Martin J, Ponçot M, Hiver JM, Bourson P, Dahoun AJ. Raman Spectrosc 2013;44(5):776–84.
[24] Peterlin A. J Mater Sci 1971;6(6):490–508.
[25] Flory PJ, Yoon DY. Nature 1978;272(5650):226–9.
[26] Pawlak A, Galeski A. Macromolecules 2008;41(8):2839–51.
[27] Rozanski A, Galeski A, Debowska M. Macromolecules 2011;44(1):20–8.
[28] Pawlak A, Galeski A. J Polym Sci Pol Phys 2010;48(12):1271–80.
[29] Pawlak A, Galeski A. Macromolecules 2005;38(23):9688–97.
[30] Wang YT, Jiang ZY, Fu LL, Lu Y, Men YF. PLoS ONE 2014;9(5):e97234.
[31] Galeski A, Bartczak Z. Macromol Symp 2003;194(1):47–62.
[32] Li JX, Cheung WL. Polymer 1998;39(26):6935–40.
[33] Cai ZW, Zhang Y, Li JQ, Xue FF, Shang YR, He XH, et al. Polymer 2012;53(7):1593–601.
[34] Xu W, Martin DC, Arruda EM. Polymer 2005;46(2):455–70.
[35] Lezak E, Bartczak Z, Galeski A. Polymer 2006;47(26):8562–74.
[36] Bao RY, Ding ZT, Liu ZY, Yang W, Xie BH, Yang MB. Polymer 2013;54(3):1259–68.
[37] Li JX, Cheung WL, Chan CM. Polymer 1999;40(8):2089–102.
[38] Li JX, Cheung WL, Chan CM. Polymer 1999;40(13):3641–56.
[39] Lotz B. Polymer 1998;39:4561–7.
[40] Pawlak A. J Appl Polym Sci 2012;125(6):4177–87.
[41] Offord GT, Armstrong SR, Freeman BD, Baer E, Hiltner A, Swinnea JS, et al. Polymer 2013;54(10):2577–89.
[42] Chu F, Yamaoka T, Ide H, Kimura Y. Polymer 1994;35(16):3442–8.
[43] Ran SF, Xu M. Chin J Polym Sci 2004;22(2):123–30.
[44] Galeski A. Prog Polym Sci 2003;28(12):1643–99.
[45] Jones AT, Aizlewood JM, Beckett DR. Makromol Chem 1964;75:134–58.
[46] Qiu J, Wang Z, Yang L, Zhao J, Niu Y, Hsiao BS. Polymer 2007;48(23):6934–47.
[47] Shi GY, Chu F, Zhou GE, Han ZW. Die Makromol Chem 1989;190(4):907–13.
[48] Ran S, Zong X, Fang D, Hsiao BS, Chu B, Phillips RA. Macromolecules 2001;34(8):2569–78.
[49] Liu G, Zhang X, Liu Y, Li X, Chen H, Walton K, et al. Polymer 2013;54(4):1440–7.
[50] Hsiao BS, Kennedy AD, Leach RA, Chu B, Harney P. J Appl Crystallogr 1997;30(6):1084–95.
[51] Butler MF, Donald AM, Ryan AJ. Polymer 1998;39(1):39–52.
[52] Butler MF, Donald AM, Ryan AJ. Polymer 1997;38(22):5521–38.
[53] Baltá-Calleja FJ, Peterlin A. J Mater Sci 1969;4(8):722–9.
[54] Peterlin A, Baltá-Calleja FJ. J Appl Phys 1969;40(11):4238–42.
[55] Butler MF, Donald AM. Macromolecules 1998;31(18):6234–49.
[56] Liu LZ, Hsiao BS, Fu BX, Ran S, Toki S, Chu B, et al. Macromolecules 2003;36(6):1920–9.
[57] Zhang X, Schneider K, Liu G, Chen J, Brüning K, Wang D, et al. Polymer 2012;53(2):648–56.
[58] Pawlak A. Polymer 2007;48(5):1397–409.
[59] Zhang X, Schneider K, Liu G, Chen J, Brüning K, Wang D, et al. Polymer 2011;52(18):4141–9.
[60] Zannetti R, Celotti G, Fichera A, Francesconi R. Die Makromol Chem 1969;128(1):137–42.
[61] Saraf RF, Porter RS. Polym Eng Sci 1988;28(13):842–51.
[62] Osawa S, Porter RS. Polymer 1994;35(3):545–50.
[63] Jolly L, Tidu A, Heizmann JJ, Bolle B. Polymer 2002;43(25):6839–51.